RSC Advances

PAPER

View Article Online
View Journal | View Issue

Cite this: *RSC Adv.*, 2021, **11**, 30046

Coordination-based vapochromic behavior of a luminescent Pt(II) complex with potassium ions†

Yasuhiro Shigeta, *[a] Ryota Nanko,[b] Shogo Amemori [acd] and Motohiro Mizuno *[acd]

Received 7th July 2021
Accepted 2nd September 2021

DOI: 10.1039/d1ra05236e

rsc.li/rsc-advances

Vapochromic Pt(II) complexes that exhibit color and luminescence changes induced by the presence of vapor molecules have drawn considerable attention because of their potential use as vapor sensors. Generally, the vapochromic responsiveness of Pt(II)-based complexes is difficult to envisage, because a typical molecular design facilitates the stabilization of a vapor-adsorbed form through weak intermolecular interactions. Herein, we investigate the vapochromic behavior of a Pt(II) complex with potassium ions, which act as vapor coordination sites, by strongly stabilizing the vapor-adsorbed form. Upon exposure to *N*,*N*-dimethylacetamide and *N*,*N*-dimethylformamide vapors, the complex exhibits crystal structural transformation with luminescence spectral changes. Crystal structural analysis indicates that the vapor molecules are coordinated to the potassium ions after vapor exposure. This study suggests the possibility of inducing Pt(II)-based vapochromic responsiveness through establishing potassium-ion-based vapor coordination sites.

Introduction

Vapochromic materials with color/luminescence changes induced by vapor molecules have attracted considerable attention because these materials facilitate the visual detection of even invisible harmful volatile organic compounds (VOCs).[1,2] Various types of vapochromic materials have been reported so far. Flexible responsive crystalline materials with a high structural order, called soft crystals, have been extensively examined in recent decades.[3] Notably, coordination compounds have been widely explored as vapochromic materials that interact with chromophores through mainly two types of mechanism.[4] Through the Type I mechanism, vapochromic materials exhibit color and luminescence changes by modifying intermolecular interactions on chromophores induced by vapor molecules.[5–22] In contrast, the Type II mechanism allows the generation of vapochromism from the direct coordination of vapor molecules to the chromophore, resulting in a change in the absorption/emission energy.[23–36] Pt(II) complexes with Pt⋯Pt interactions (Type I mechanism) are promising candidates of vapochromic materials. Pt(II) complexes tend to form a one-dimensional stacking structure through the overlapping of the $5d_{z^2}$ orbitals of the Pt(II) ions. In this state, characteristic absorptions/emissions derived from intermolecular Pt⋯Pt interactions (*e.g.*, metal–metal-to-ligand charge transfer; MMLCT) are observed. Pt(II) complexes undergo crystal structure transformation upon the adsorption of vapor molecules; this transformation induces the color and luminescence changes, which are caused by the high dependence of MMLCT energy on the metallophilic interaction degree.[37,38]

However, even for the most reported vapochromic Pt(II) complexes with Type I mechanism, the rationale for their vapor responsiveness from the molecular design stage has not been elucidated. This is probably because the stabilization of adsorbed vapor molecules on almost all vapochromic Pt(II) complexes is achieved by relatively weak intermolecular interactions, such as hydrogen bonding.[6,7,9–12,14,15,18–22] Thus, the vapor-adsorbed crystal structure was not effectively stabilized, making it difficult to determine whether vapor adsorption occurred. Conversely, it is a common strategy for non-Pt(II) vapochromic complexes to provide a strong binding site, such as a coordination site, for vapor molecules to bind with the host molecules (including Type II mechanism).[23–36] Such binding sites would strongly stabilize the vapor-adsorbed state and probably enable us to clarify the vapor adsorption behavior. To extend this strategy to Pt(II) complexes, we focused on alkali metal ions, because these ions would act as coordination sites and can be introduced easily into the metal complex.

[a]*NanoMaterials Research Institute, Kanazawa University, Kanazawa 920-1192, Japan. E-mail: y-shigeta@se.kanazawa-u.ac.jp; mizuno@se.kanazawa-u.ac.jp*

[b]*School of Chemistry, College of Science and Engineering, Kanazawa University, Kanazawa, 920-1192, Japan*

[c]*Graguate School of Natural Science and Technology, Kanazawa University, Kanazawa 920-1192, Japan*

[d]*Institute of Frontier Science Initiative, Kanazawa University, Kanazawa 920-1192, Japan*

† Electronic supplementary information (ESI) available: ^{1}H NMR spectrum, thermogravimetric analysis and emission spectrum. CCDC 2084817 and 2084818. For ESI and crystallographic data in CIF or other electronic format see DOI: 10.1039/d1ra05236e

There have been limited reports on vapochromic Pt(II) complexes with alkali metal ions. For instance, Sicilia *et al.* reported the vapochromic behavior of luminescent Pt(II) complexes, $[K(H_2O)][Pt(CN)_2(ppy)]$ (ppy = 2-phenylpyridinato) and $[K(H_2O)][Pt(CN)_2(bzq)]$ (bzq = 7,8-benzoquinolinato), with potassium ions.[39] Both samples exhibited vapochromism upon exposure to H_2O vapor and drying. Moreover, $[K(H_2O)][Pt(CN)_2(bzq)]$ exhibited vapochromic behavior after exposure to various organic vapor molecules. Further, the H_2O vapor induced vapochromic behaviors of $[K(H_2O)][M(CN)_2(ppy)]$ and $[K(H_2O)][M(CN)_2(bzq)]$ (M = Pt or Pd) were further investigated using several experimental techniques.[40] Single crystal X-ray structural analysis of $[K(H_2O)][Pt(CN)_2(ppy)]$ revealed that potassium ions were coordinated by cyanide ligands and water molecules. Furthermore, X-ray diffraction and TG measurements indicated that the H_2O molecule showed coordination(adsorption)- and dissociation-based vapochromic behavior. In contrast, Kobayashi *et al.* reported the vapochromic behavior of a sodium-ion-containing Pt(II) complex, $Na_2[Pt(CN)_2(dcbpy)]\cdot 2H_2O$ (dcbpy = 2,2′-bipyridine-4,4′-dicarboxylate).[41] X-ray diffraction measurements revealed that the H_2O molecules were coordinated to the sodium ion. However, this complex did not show vapor-coordination-based vapochromic behavior; it displayed vapor-induced structural transformation from an amorphous to a crystalline form without changing the molecular composition. These reports indicate the possibility of coordination-based vapochromic behavior. However, the effect of vapor molecules coordination with alkali metal ions is still unclear and reported coordination-based vapochromic behavior has been reported to be limited to water molecule. Therefore, further studies are required to investigate the possibility of coordination-based vapochromism in Pt(II) complexes with direct vapor coordination sites.

To confer coordination-based vapor responsiveness, structural flexibility is favorable to allow for structural transformation to various crystals upon the coordination of vapor molecules. To fulfill this demand, we considered halogen atoms because they have been known to interact with other atoms through hydrogen bonding, halogen bonding, and halogen–halogen interactions.[42–44] In particular, halogen–halogen interactions have been known to induce versatile geometrical conformations. Because of the structural flexibility imparted by halogen atoms, they can be applied in the formation of various crystal structures and can enable alkali metal ions to function as vapor coordination sites.

Herein, we have synthesized a new Pt(II) complex with K^+ ions and chlorides, $K[Pt(CN)_2(ppyCl_2)]$ (**1**; $ppyCl_2$ = 2-(3-chlorophenyl)-4-chloropyridinato; Scheme 1) and investigated its crystal structure and vapochromic behavior. Complex **1** exhibited vapochromic luminescence upon exposure to *N*,*N*-dimethylacetamide (DMA) and *N*,*N*-dimethylformamide (DMF) vapors accompanied by the coordination of vapor molecules, as suggested by emission spectroscopy and X-ray diffraction (XRD) analysis.

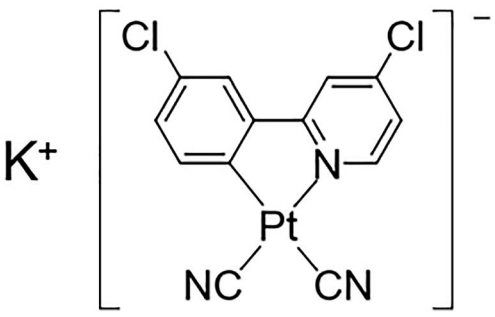

Scheme 1 Molecular structure of **1**, $K[Pt(CN)_2(ppyCl_2)]$ ($ppyCl_2$ = 2-(3-chlorophenyl)-4-chloropyridinato).

Experimental section

General procedures

All commercially available materials were used as received. 2-Bromo-4-chloropyridine, 3-chlorophenylboronic acid and $Pd(PPh_3)_4$ was purchased from Tokyo Chemical Industry Co. Ltd. The other materials were purchased from FUJIFILM Wako Pure Chemical Corporation. All experiments were conducted under ambient conditions, unless stated otherwise. ^{1}H NMR spectra were recorded using a JEOL ECS400 spectrometer. Elemental analysis was conducted at the Advanced Science Research Center at Kanazawa University.

Synthesis of 2-(3-chlorophenyl)-4-chloropyridine ($HppyCl_2$)

A two-neck round-bottom flask was charged with Na_2CO_3 (2.0 g, 19 mmol) and a solvent mixture of H_2O (17 mL), methanol (68 mL), and toluene (85 mL). 2-Bromo-4-chloropyridine (1.92 g, 10 mmol) was added to the flask and N_2 was bubbled through the mixture for 30 min. After purging the flask with N_2, 3-chlorophenylboronic acid (2.34 g, 15 mmol) and $Pd(PPh_3)_4$ (90 mg, 0.078 mmol) were added. The resulting mixture was heated at 378 K while stirring for 1.5 h under N_2 atmosphere. The resulting mixture was subsequently cooled to 298 K and then filtered. H_2O (100 mL) was then added to the filtrate, which was subsequently extracted with CH_2Cl_2 (50 mL × 3). The organic layers were collected; they were dried over Na_2SO_4 and evaporated to dryness. The crude product was purified by silica gel column chromatography (eluent : hexane/ethyl acetate = 10 : 1) to obtain the target ligand as a white powder. Yield: 1.41 g, 63%. ^{1}H NMR (400 MHz, $CDCl_3$, δ): 8.59 (d, 1H, J = 5.0 Hz), 8.00 (m, 1H), 7.84 (m, 1H), 7.72 (d, 1H, J = 1.8 Hz), 7.42 (d, 2H), 7.28 (ddd, 1H, J = 5.5 Hz, 1.8 Hz, 0.9 Hz).

Synthesis of $K[Pt(ppyCl_2)(CN)_2]$ (1)

Objective complex **1** was synthesized based on a previously published method with a slight modification.[39] The reported synthetic method of $K[Pt(CN)_2(ppy)]$ was divided into three steps along with the isolation of precursors. Compound **1** was synthesized without the isolation of precursors because of the difficulty for isolation of the complexes in each step. K_2PtCl_4 (415 mg, 1.0 mmol) was dissolved in H_2O (15 mL) and $HppyCl_2$

(243 mg, 1.0 mmol) was dissolved in 2-ethoxyethanol (20 mL). These solutions were combined in a two-neck round-bottom flask, and the resulting mixture was bubbled with N_2 for 30 min. The flask was purged with N_2, heated at 343 K for 2 h, and subsequently heated at 373 K for 19 h under a N_2 atmosphere. The mixture was then cooled to 298 K, and H_2O (50 mL) was added. The resulting solid was filtered and washed with H_2O, ethanol, and CH_2Cl_2 to obtain a dark green solid. The solid was then added to MeCN (100 mL). $AgClO_4$ (456 mg per obtained solid, 1000 mg) was added to the mixture, which was stirred overnight under dark conditions. After the reaction, the mixture was filtered through Celite, and the filtrate was evaporated to dryness. The resulting dark green solid was suspended in Et_2O and filtered. The obtained solid was washed with Et_2O to obtain a green solid. The obtained solid (590 mg) was suspended in MeOH (100 mL). KCN (128 mg, 1.97 mmol) was added to the mixture, and the resulting suspension was stirred for 3 h at 298 K. The obtained mixture was filtered through Celite and evaporated to dryness. The solid was finally suspended in CH_2Cl_2, filtered and subsequently washed with CH_2Cl_2 and H_2O to obtain as-synthesized **1**, which was used as described in the "Molecular composition" section. The solid product was dried under vacuum and heated at 473 K for 2 h, and cooled to 298 K under air to obtain **1·0.3H$_2$O** as a yellow solid. Yield: 321 mg, 30%. ^{1}H NMR (400 MHz, DMSO-d_6, δ) 9.15 (d, 1H), 8.38 (d, 1H), 7.94 (d, 1H), 7.86 (d, 1H), 7.61 (dd, 1H), 7.17 (dd, 1H). Elemental analysis, found: C, 30.19; H, 1.45; N, 8.09. Calc. for $KPtCl_2C_{13}N_3H_6 \cdot 0.3(H_2O)$ (**1·0.3H$_2$O**): C, 30.34; H, 1.29; N, 8.16%.

Single crystal preparation

DMA containing single crystal (**1·3DMA**) was obtained by diethyl ether vapor diffusion to a DMA solution of **1** (2.0 mg in 1.0 mL) in a refrigerator. DMF containing single crystal (**1·0.75DMF**) was obtained by diethyl ether vapor diffusion through a DMF solution of **1** (2.1 mg in 1.1 mL) in a refrigerator.

Vapor responsiveness experiment

1 was added to a test tube and a vial was added a vapor source. Then the test tube was placed into vial and sealed. The vial was left in the incubator.

Luminescence spectrum

The luminescence spectrum for each sample was collected using a Hitachi F-2500 spectrofluorometer. The measured sample was then charged into a glass capillary. The typical slit width for both excitation and emission was 10 nm.

Absorption spectrum

The absorption spectrum in the solution state was collected using a JASCO V-750 spectrophotometer.

Powder XRD study

Powder XRD analysis was conducted on a Bruker D8 Advance Eco diffractometer using Cu Kα radiation.

Thermogravimetric analysis

Thermogravimetric analysis (TGA) of each sample was conducted using a Rigaku Thermo Plus EVO2 TG-8121 analyzer. The heating rate was 5 K min^{-1} in all measurements.

Single crystal X-ray structural analysis

Single crystal X-ray measurements were conducted using a Bruker D8 Venture diffractometer with Cu Kα radiation. Each single crystal was mounted on MicroMount coated with Parabar 10312 oil. The measurement temperature was controlled using a N_2-flow type temperature controller. The diffraction data were collected and processed using the Bruker APEX III software. The structures were solved by the intrinsic phasing method using SHELXT.[45] Structural refinement was conducted using the full-matrix least-squares method with SHELXL.[45] Non-hydrogen atoms were refined anisotropically, and all hydrogen atoms were refined using a riding model. The calculations were conducted using the Olex2 software package.[46] Full crystallographic data are deposited with the Cambridge Crystallographic Data Centre (CCDC 2084817 and 2084818).

Results and discussion

Crystal structures

To examine the possibility of vapor-molecule-coordination-induced vapochromic behavior, firstly, we verified the ability of the complex to undergo recrystallization under several conditions, and succeeded in obtaining DMA- and DMF-coordinated crystal structures. Fig. 1 illustrates the crystal

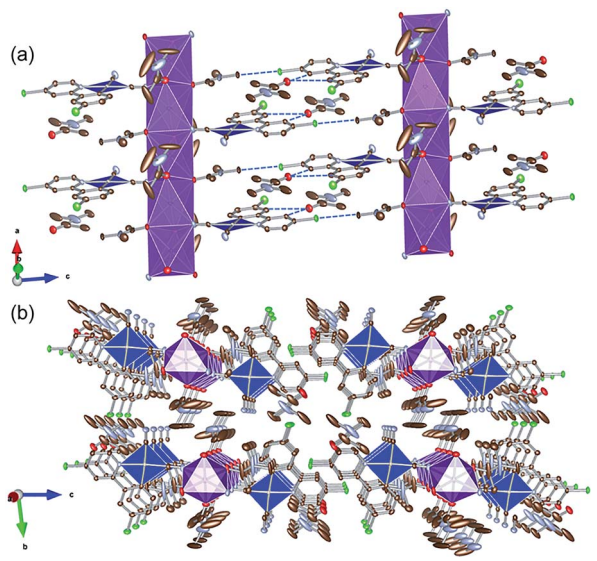

Fig. 1 (a) Column-like structure and (b) packing crystal structure of **1·3DMA**. Hydrogen atoms are omitted for clarity. One of the two disordered DMA molecules is illustrated. Gray, light blue, red, green, and purple ellipsoids show the C, N, O, Cl, and K atoms, respectively. The blue and purple polyhedra indicate the Pt and K centers, respectively. Displacement parameters are drawn at 50% probability level. These pictures were illustrated using the VESTA computer program.[47]

structure of the DMA-coordinated form, **1·3DMA**. The crystallographic parameters, selected bond lengths and the atom labels around the Pt(II) ions are shown in Tables 1, 2 and Fig. S1,† respectively. The crystal contained a crystallographically independent $[Pt(CN)_2(ppyCl_2)]^-$ ion, one K^+ ion, and three DMA molecules. All the DMA molecules were positionally disordered between the two sites. The Pt(II) center showed a square planar coordination geometry and was coordinated by one $ppyCl_2$ ligand and two cyanido ligands. The bond lengths between the Pt atom and the two cyanido ligands are marginally different from each other [1.942(4) Å and 2.027(3) Å]. This difference could be due to the *trans* influence of the σ-donating carbon atom of the $ppyCl_2$ ligand on the longer bond. Moreover, one of the N atoms on the cyanido ligand was coordinated to the K^+ ion. The K^+ ion was further coordinated by four adjacent DMA molecules. As a result, a one-dimensional column-like structure was formed along the *a*-axis through the anionic Pt(II) complex, K^+ ion, and coordinated DMA molecules (Fig. 1(a)). Another DMA molecule was weakly bound by CH···O-type hydrogen bonding [3.354(5) Å and 3.256(4) Å] between the $ppyCl_2$ ligand (C5 and C8) and the C=O moiety of DMA. In the column structure, Pt(II) complexes were separated by a DMA molecule between two adjacent Pt complexes, indicating negligible Pt···Pt interactions. In fact, the shortest intermolecular Pt···Pt distances were estimated to be 7.4967(3) Å, which is longer than twice the van der Waals radius of the Pt atom (3.5 Å). These columns interacted through CH···Cl hydrogen bonding (3.299(6) Å) between the DMA molecule and $ppyCl_2$ ligand.

Fig. 2 illustrates the crystal structure of the DMF-coordinated form, **1·0.75DMF**. The crystallographic parameters, selected bond lengths, and atom labels around Pt(II) ions are shown in Tables 1, 2 and Fig. S1,† respectively. The flack parameter value [0.42(1)] suggested twinning by inversion. The crystal comprised four crystallographically independent $[Pt(CN)_2(ppyCl_2)]^-$ ions, four K^+ ions, and three DMF molecules. Tables 2

Table 1 Crystal parameters and refinement results of **1·3DMA** and **1·0.75DMF**

Complex	**1·3DMA**	**1·0.75DMF**
T/K	90	90
Formula	$C_{23}H_{33}Cl_2KN_6O_3Pt$	$C_{15.25}H_{11.25}Cl_2KN_{3.75}O_{0.75}Pt$
Formula weight	746.63	564.12
Crystal system	Triclinic	Monoclinic
Space group	$P\bar{1}$	*Cc*
a/Å	7.4967(2)	41.7895(9)
b/Å	10.2891(3)	8.5044(2)
c/Å	20.1177(5)	21.2104(4)
α/°	79.821(1)	90
β/°	87.171(1)	107.837(1)
γ/°	74.152(1)	90
V/Å^3	1469.29(7)	7175.7(3)
Z	2	16
D_{cal}/g cm^{-3}	1.742	2.089
Reflections collected	12 451	27 578
Unique reflections	5622	11 342
GOF	1.051	1.064
Flack parameter	—	0.42(1)
R_{int}	0.0276	0.0470
R [$I > 2.00\sigma(I)$]	0.0252	0.0335
R_w[a]	0.0633	0.0850

[a] $R_w = \{\Sigma[w(F_o^2 - F_c^2)^2]/\Sigma w(F_o^2)^2\}^{1/2}$.

Table 2 Selected bond lengths and intermolecular Pt···Pt distances of **1·3DMA** and **1·0.75DMF** at 90 K

Complex	**1·3DMA**	**1·0.75DMF**
Pt1–N1	2.070(3) Å	2.08(1) Å
Pt1–C1	2.027(3) Å	2.01(1) Å
Pt1–C12	1.942(4) Å	1.97(1) Å
Pt1–C13	2.027(3) Å	2.01(1) Å
Pt2–N4	—	2.04(1) Å
Pt2–C14	—	2.05(1) Å
Pt2–C25	—	1.93(2) Å
Pt2–C26	—	2.03(1) Å
Pt1···Pt1	7.4967(3) Å	—
Pt1···Pt2	—	3.4765(6) Å, 6.7976(7) Å

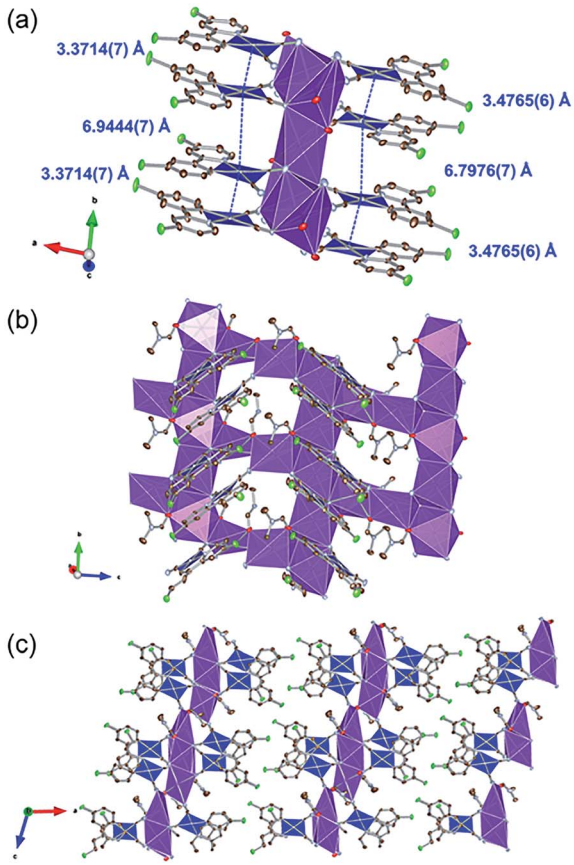

Fig. 2 (a) Stacking structure, (b) packing structure around K^+ ion and (c) crystal packing of **1·0.75DMF**. Hydrogen atoms are omitted for clarity. Gray, light blue, red, and green ellipsoids show the C, N, Cl, and O atoms, respectively. The blue and purple polyhedra indicate Pt and K centers, respectively. Displacement parameters are drawn at 50% probability level. These pictures were illustrated using the VESTA computer program.[47]

and S1† highlight the bond lengths around the Pt(II) ions being comparable to that of **1·3DMA**. This indicates that included DMA and DMF molecules marginally affects the coordination environment around the Pt(II) center. In this crystal structure, Pt(II) complexes were stacked along the *b*-axis. The distances between the two Pt(II) ions were estimated to be 3.4765(6) Å and 6.7976(7) Å (for Pt1 and Pt2) and 3.3714(7) Å and 6.9444(7) Å (for Pt3 and Pt4), suggesting an effective Pt···Pt interaction between adjacent two Pt(II) complexes. Similar to **1·3DMA**, the Pt(II) complex in **1·0.75DMF** was coordinated to the K^+ ion with the N atoms of the cyanide ligand. All DMF molecules were coordinated to K^+ ions through the oxygen atoms of the C=O moieties. Three out of four K^+ ions were coordinated by two neighboring DMF molecules and four cyanide ligands from four crystallographically independent $[Pt(CN)_2(ppyCl_2)]^-$ anions, while the other K^+ ion was coordinated by four adjacent $[Pt(CN)_2(ppyCl_2)]^-$ anions. Consequently, the complex formed a two-dimensional sheet-like structure in the *bc* plane, as displayed in Fig. 2(c). The sheet-like structures were formed through halogen–halogen interactions between two Cl atoms [3.302(5) Å and 3.478(7) Å]. These crystal structure with different interaction modes of Cl atoms suggest that structural flexibility was conferred by Cl atom modification.

Molecular composition

Before examining the vapor responsiveness, determination of the molecular composition would be favorable to explore the possibility of vapor-coordination-based vapochromic behavior. Alkali metal ions often include solvent molecules coordinated to them making it is unclear whether the coordinated molecules affect the vapochromic behavior. To determine the molecular composition, thermogravimetric (TG) analysis (Fig. 3) and ^{1}H NMR measurements (Fig. S2†) were conducted. Upon heating, the TG curve of as-synthesized **1** showed a 2.6% weight loss at 473 K. Additionally, the ^{1}H NMR spectrum in DMSO-d_6 of as-synthesized **1** showed no assignable peaks to solvents used during synthesis and purification (MeOH and CH_2Cl_2), with the exception of H_2O. Therefore, the weight loss was assigned to desorption of H_2O from the as-synthesized **1**. The weight loss value was close to that of the H_2O desorption from **1·0.8H$_2$O** (2.7%). Following TG analysis at 473 K, the sample composition was further confirmed by elemental analysis (see Experimental section). The obtained value suggests the molecular composition of the sample to be in the range of **1·0.2H$_2$O** to **1·0.7H$_2$O** (Table S2†), despite the H_2O molecules being desorbed through heating. To elucidate this observation, further TG measurements were performed. The TG curve (red line in Fig. 3) showed a 1.1% weight loss, which corresponded to the **1·0.3H$_2$O** (1.0%). These measurements indicate that **1** changed its molecular composition by re-adsorption of H_2O molecules under ambient conditions even after dehydration through heating.

Vapor responsiveness

The crystal structures of **1** coordinated with DMA and DMF, **1·3DMA** and **1·0.75DMF**, respectively, have been discussed in the previous sections. Powder XRD analysis was conducted to elucidate whether vapor-induced structural changes occur. Fig. 4 shows the changes in the powder XRD pattern of **1·0.3H$_2$O** (the hydration number is estimated from TG measurement and elemental analysis) upon DMA and DMF

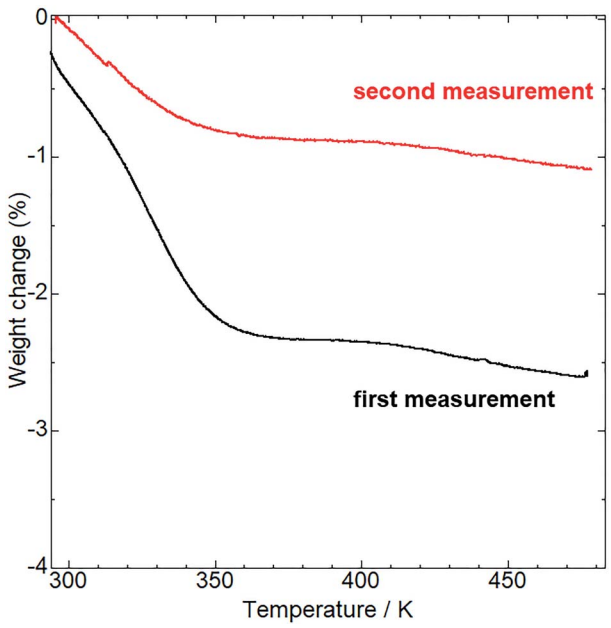

Fig. 3 TG analysis of the as-synthesized (first measurement, black line) and aged (second measurement, red line) **1**. The aged sample was preserved under ambient conditions for a week after the first measurement.

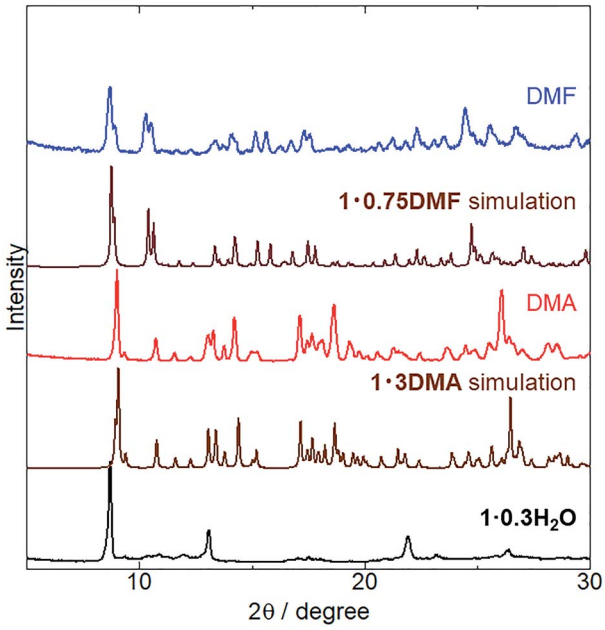

Fig. 4 XRD patterns of as-synthesized (black) **1·0.3H$_2$O** exposed to DMA vapor (red) at 298 K for 5 days and to DMF vapor (blue) at 278 K for 1 day. Simulated patterns of **1·3DMA** and **1·0.75DMF** are also displayed (brown).

vapor exposure. Although the crystal structure of **1·0.3H$_2$O** has not been determined, the XRD pattern of **1·0.3H$_2$O** shows some discernable sharp peaks, suggesting the presence of an ordered crystal structure. After exposure to DMA vapor at 298 K and DMF vapor at 278 K, the XRD pattern of **1·0.3H$_2$O** changed considerably. The obtained patterns were similar to simulated those of **1·3DMA** and **1·0.75DMF**, indicating a vapor-induced structural transformation from **1·0.3H$_2$O** to **1·3DMA** and **1·0.75DMF**. Although we also tried the vapochromic test of DMF at 298 K, **1** transformed to the other phase; however, the phase was completely different from **1·0.75DMF**. Lattice constant refinement fitting results (Fig. S3†) showed that there was no obvious extra peak, which also indicates the transformations. The obtained lattice constants (Table S3†) were slightly larger than those of single crystals, likely because of the measurement temperature: single crystal X-ray diffraction measurements were conducted at 90 K, whereas the powder X-ray diffraction measurement data were collected at 293 K. The molecular composition of these vapor-exposed samples was confirmed by thermogravimetric analysis (Fig. S4 and S5†). Upon heating, the DMA- and DMF-vapor-exposed samples lost 33% and 9.7% of their weight, which is in agreement with the weight loss after solvate molecule desorption in **1·3DMA** (35%) and **1·0.75DMF** (9.7%). Slight discrepancies in the weight loss value for the DMA-vapor-exposed sample may be due to DMA desorption during sample preparation. Despite the higher boiling point of DMA (438 K) than that of DMF (426 K), guest molecule desorption from **1·3DMA** (303 K) started at a lower temperature than that of **1·0.75DMF** (323 K). This discrepancy is likely due to the presence of non-coordinated guest molecules in **1·3DMA**, which is relatively unstable and easily desorbed. These results suggest the stabilization of the guest molecule by coordination with the potassium ion. Vapor adsorption for each sample was also confirmed by ^{1}H NMR spectra (Fig. S6 and S7†). The spectra showed new peaks which corresponded to DMA and DMF, suggested that the observed weight loss from TG analysis can be assigned to the desorption of solvate guest molecules. Although the initial **1** included H$_2$O molecules, **1·0.3H$_2$O** transformed to **1·3DMA** and **1·0.75DMF**, which comprised no H$_2$O molecules after exposure to DMA and DMF vapors. These results demonstrate that the presence of H$_2$O molecules in the initial **1·0.3H$_2$O** negligibly affects the structural transformation induced by exposure to DMA and DMF vapors.

Subsequently, we examined the vapochromic luminescence behavior of **1** arising from the vapor-induced structural transformations, as confirmed by XRD analysis. Before the measurement, we compared the color of **1** in solutions and **1·3DMA** and **1·0.75DMF** crystals (Fig. S8†) to elucidate the coordination effects of the guest molecules. **1** exhibited similar color in solutions of DMA and DMF. This result was also confirmed by absorption spectra; **1** exhibited almost same absorption spectra in these solvents (Fig. S9†). Therefore, coordination of the guest molecules to the potassium ion and/or surrounding environment hardly affected the electronic states of **1**. Both the color of DMA solutions of **1** and **1·3DMA** crystals showed similar pale yellow. On the other hand, the color of the DMF solution of **1** (pale yellow) was different from

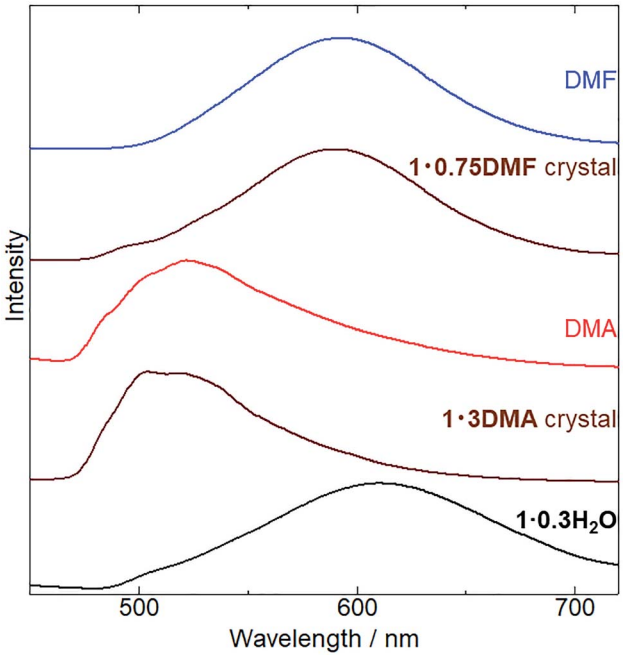

Fig. 5 Changes in emission spectra (λ_{ex} = 400 nm) of **1·0.3H$_2$O** (black), **1** exposed to DMA vapor (red) at 298 K for 5 days and to DMF vapor (blue line) at 278 K for 1 day. Emission spectra of **1·3DMA** and **1·0.75DMF** single crystals (brown) are also shown for comparison.

that of the **1·0.75DMF** crystal (orange yellow). Therefore, the color of the crystal would be dominated by intermolecular interactions, such as Pt···Pt interactions. Fig. 5 shows the emission spectrum of **1·0.3H$_2$O** upon exposure to DMA and DMF vapors, and the images of these vapor exposed samples were also shown in Fig. S10.† The initial **1·0.3H$_2$O** exhibited a broad emission spectrum centered at 610 nm. The emission spectrum of a DMA solution of **1** was used to assign the origin of the emission (Fig. S6†). This measurement illustrated that monomer of **1** exhibited a 527 nm emission with vibronic progression, which can be assigned to the ^{3}LC emission derived from the ligands. These results suggest that an effective Pt···Pt interaction exists in the initial state and that the emission is assigned to ^{3}MMLCT luminescence. After exposure to DMA vapor for 5 days, the spectrum changed from a broad emission spectrum centered at 610 nm to that with an obscure structure at 523 nm. The emission spectrum of DMA-vapor-exposed **1·0.3H$_2$O** was almost identical to that of **1·3DMA** single crystals, indicating crystal structural transformation from **1·0.3H$_2$O** to **1·3DMA**, which is in agreement with the XRD analysis results. **1·3DMA** was shown to undergo negligible Pt···Pt interactions, which are expected to induce emissions from monomeric species. Furthermore, both DMA-exposed **1** and the solution state of **1** exhibited emissions in around the same wavelength region. Based on these results and those previously reported on related cyclometalated Pt(II) complexes,[39,48–50] we tentatively assigned the emission to a mixed ^{3}MLCT/^{3}LC emission from monomer **1**. Consequently, after DMF vapor exposure, the broad emission band of **1·0.3H$_2$O** slightly shifted from 610 nm to 590 nm, almost corresponding to the emission

maxima of the **1·0.75DMF** single crystal. As a consequence of the effective intermolecular Pt···Pt interaction, determined through single crystal X-ray structural analysis, the emission from the DMF-vapor-exposed sample could be assigned to the ^{3}MMLCT transition.

Conclusions

We synthesized a luminescent Pt(II) complex (**1**) with potassium ions, which act as vapor coordination sites. Single crystal X-ray structural analysis of the DMA-coordinated complex, **1·3DMA**, which recrystallized from diethyl ether vapor diffusion to the DMA solution of **1**, emphasize that two out of three DMA molecules were coordinated to the K^+ ion and formed a one-dimensional column-like crystal structure without intermolecular Pt···Pt interactions. These columns interacted with each other through CH···Cl hydrogen bonding between the DMA molecule and $ppyCl_2$ ligand. Consequently, X-ray structural analysis of **1·0.75DMF** revealed that all DMF molecules coordinated to the K^+ ion and formed a two-dimensional sheet-like structure through effective intermolecular Pt···Pt interactions between adjacent dimers. The sheet-like structures interacted *via* halogen–halogen interactions between Cl atoms. Upon exposure to DMA and DMF vapors, **1** exhibited vapor-induced structural transformation from **1·0.3H$_2$O** to **1·3DMA** and **1·0.75DMF**, respectively. TG analysis comparison of these forms revealed that **1·3DMA** is more unstable than **1·0.75DMF**, despite the higher boiling point of DMA compared to DMF. This behavior likely arises from the non-coordinated DMA molecule in **1·3DMA**, which is relatively unstable and suitable for desorption. On the other hand, detailed *in situ* X-ray measurements for $[K(H_2O)][Pt(CN)_2(bzq)]$ and $[K(H_2O)][Pt(CN)_2(ppy)]$, reported by Caliandro *et al.*, suggested that intermolecular metallophilic and π–π interactions are crucial to the vapochromic process in the desorption of H_2O molecules.[40] Our results suggest that the interaction between guest molecules and coordination sites is also important for vapochromic behavior (desorption of the guest molecules). After DMA vapor exposure, **1** exhibited emission centered at 523 nm, which was tentatively assigned to the mixed ^{3}MLCT/^{3}LC emission from the Cl_2ppy ligand. In contrast, a broad emission centered at 590 nm was observed after DMF vapor exposure, which was assigned to the ^{3}MMLCT emission due to effective intermolecular Pt···Pt interactions. This study demonstrates that K^+ ion and halogen atom modifications of Pt(II) complexes are a promising approach to confer vapochromic responsiveness to Pt(II) complexes through coordination of vapor molecules.

Conflicts of interest

There are no conflicts of interest to declare.

Acknowledgements

This research was supported by JSPS KAKENHI grant numbers JP19K23649 and JP20H04666.

Notes and references

1 A. Kobayashi and M. Kato, *Eur. J. Inorg. Chem.*, 2014, 4469.
2 P. Minei and A. Pucci, *Polym. Int.*, 2016, **65**, 609.
3 M. Kato, H. Ito, M. Hasegawa and K. Ishii, *Chem.–Eur. J.*, 2019, **25**, 5105.
4 O. S. Wenger, *Chem. Rev.*, 2013, **113**, 3686.
5 C. E. Buss and K. R. Mann, *J. Am. Chem. Soc.*, 2002, **124**, 1031.
6 T. J. Wadas, Q.-M. Wang, Y.-J. Kim, C. Flaschenreim, T. N. Blanton and R. Eisenberg, *J. Am. Chem. Soc.*, 2004, **126**, 16841.
7 S. C. F. Kui, S. S.-Y. Chui, C.-M. Che and N. Zhu, *J. Am. Chem. Soc.*, 2006, **128**, 8297.
8 S. M. Drew, L. I. Smith, K. A. McGee and K. R. Mann, *Chem. Mater.*, 2009, **21**, 3117.
9 S. J. Choi, J. Kuwabara, Y. Nishimura, T. Arai and T. Kanbara, *Chem. Lett.*, 2012, **41**, 65.
10 S. D. Taylor, A. M. Norton, R. T. Hart Jr, M. K. Abdolmaleki, J. A. Krause and W. B. Connick, *Chem. Commun.*, 2013, **49**, 9161.
11 R. Zhang, Z. Liang, A. Han, H. Wu, P. Du, W. Lai and R. Cao, *CrystEngComm*, 2014, **16**, 5531.
12 N. Kitani, N. Kuwamura, T. Tsuji, K. Tsuge and T. Konno, *Inorg. Chem.*, 2014, **53**, 1949.
13 Z.-P. Zhang, T. Wu, J. Liu, J.-X. Zhang, C.-H. Li and X.-Z. You, *J. Mater. Chem. C*, 2014, **2**, 184.
14 A. Kobayashi, S. Oizumi, Y. Shigeta, M. Yoshida and M. Kato, *Dalton Trans.*, 2016, **45**, 17485.
15 Y. Shigeta, A. Kobayashi, T. Ohba, M. Yoshida, T. Matsumoto, H.-C. Chang and M. Kato, *Chem.–Eur. J.*, 2016, **22**, 2682.
16 B. Jiang, J. Zhang, J.-Q. Ma, W. Zheng, L.-J. Chen, B. Sun, C. Li, B.-W. Hu, H. Tan, X. Li and H.-B. Yang, *J. Am. Chem. Soc.*, 2016, **138**, 738.
17 Y. Li, L. Chen, Y. Ai, E. Y.-H. Hong, A. K.-W. Chan and V. W.-W. Yam, *J. Am. Chem. Soc.*, 2017, **139**, 13858.
18 M. J. Bryant, J. M. Skelton, L. E. Hatcher, C. Stubbs, E. Madrid, A. R. Pallipurath, L. H. Thomas, C. H. Woodall, J. Christensen, S. Fuertes, T. P. Robinson, C. M. Beavers, S. J. Teat, M. R. Warren, F. Pradaux-Caggiano, A. Walsh, F. Marken, D. R. Carbery, S. C. Parker, N. B. Mckeown, R. Malpass-Evans, M. Carta and P. R. Raithby, *Nat. Commun.*, 2017, **8**, 1800.
19 Y. Shigeta, A. Kobayashi, M. Yoshida and M. Kato, *Cryst. Growth Des.*, 2018, **18**, 3419.
20 A. Kobayashi, N. Yamamoto, Y. Shigeta, M. Yoshida and M. Kato, *Dalton Trans.*, 2018, **47**, 1548.
21 K. Ohno, Y. Kusano, S. Kaizaki, A. Nagasawa and T. Fujihara, *Inorg. Chem.*, 2018, **57**, 14159.
22 J. Kang, J. Ni, M. Su, Y. Li, J. Zhang, H. Zhou and Z.-N. Chen, *ACS Appl. Mater. Interfaces*, 2019, **11**, 13350.
23 B. Li, R.-J. Wei, J. Tao, R.-B. Huang, L.-S. Zheng and Z. Zheng, *J. Am. Chem. Soc.*, 2010, **132**, 1558.
24 S. H. Lim, M. M. Olmstead and A. L. Balch, *Chem. Sci.*, 2013, **4**, 311.

25 R. J. Roberts, D. Le and D. B. Leznoff, *Chem. Commun.*, 2015, **51**, 14299.
26 T. Hayashi, A. Kobayashi, H. Ohara, M. Yoshida, T. Matsumoto, H.-C. Chang and M. Kato, *Inorg. Chem.*, 2015, **54**, 8905.
27 T. Tsukamoto, R. Aoki, R. Sakamoto, R. Toyoda, M. Shimada, Y. Hattori, Y. Kitagawa, E. Nishibori, M. Nakano and H. Nishihara, *Chem. Commun.*, 2017, **53**, 9805.
28 L. G. Beauvais, M. P. Shores and J. R. Long, *J. Am. Chem. Soc.*, 2000, **122**, 2763.
29 N. Baho and D. Zargarian, *Inorg. Chem.*, 2007, **46**, 299.
30 E. J. Fernández, J. M. López-de-Luzuriaga, M. Monge, M. E. Olmos, R. C. Puelles, A. Laguna, A. A. Mohamed and J. P. Fackler Jr, *Inorg. Chem.*, 2008, **47**, 8069.
31 C. E. Strasser and V. J. Catalano, *J. Am. Chem. Soc.*, 2010, **132**, 10009.
32 I. V. Oliveri, G. Malandrino and S. D. Bella, *Inorg. Chem.*, 2014, **53**, 9771.
33 P. Kar, M. Yoshida, Y. Shigeta, A. Usui, A. Kobayashi and M. Kato, *Angew. Chem., Int. Ed.*, 2017, **56**, 2345.
34 H. Oraha, T. Ogawa, M. Yoshida, A. Kobayashi and M. Kato, *Dalton Trans.*, 2017, **46**, 3755.
35 A. S. Sergeenko, J. S. Ovens and D. B. Leznoff, *Inorg. Chem.*, 2017, **56**, 7870.
36 S. Kondo, N. Yoshimura, M. Yoshida, A. Kobayashi and M. Kato, *Dalton Trans.*, 2020, **49**, 16946.
37 W. B. Connick, L. M. Henling, R. E. Marsh and H. B. Gray, *Inorg. Chem.*, 1996, **35**, 6261.
38 M. Kato, C. Kosuge, K. Morii, J. S. Ahn, H. Kitagawa, T. Mitani, M. Matsushita, T. Kato, S. Yano and M. Kimura, *Inorg. Chem.*, 1999, **38**, 1638.
39 J. Forniés, S. Fuertes, J. A. López, A. Martín and V. Sicilia, *Inorg. Chem.*, 2008, **47**, 7166.
40 B. D. Belviso, F. Martin, S. Fuertes, V. Sicilia, R. Rizzi, R. Ciriaco, C. Cappuccino, E. Dooryhee, A. Falcicchio, L. Maini, A. Altomare and R. Caliandro, *Inorg. Chem.*, 2011, **60**, 6349.
41 A. Kobayashi, T. Yonemura and M. Kato, *Eur. J. Inorg. Chem.*, 2010, 2465.
42 L. C. Gilday, S. W. Robinson, T. A. Barendt, M. J. Langton, B. R. Mullaney and P. D. Beer, *Chem. Rev.*, 2015, **115**, 7118.
43 G. Cavallo, P. Metrangolo, R. Milani, T. Pilati, A. Priimagi, G. Resnati and G. Terraneo, *Chem. Rev.*, 2016, **116**, 2478.
44 J. Teyssandier, K. S. Mali and S. De Feyter, *ChemistryOpen*, 2020, **9**, 225.
45 G. M. Sheldrick, *Acta Crystallogr., Sect. A: Found. Crystallogr.*, 2008, **64**, 112.
46 O. V. Dolomanov, L. J. Bourhis, R. J. Gildea, J. A. K. Howard and H. Puschmann, *J. Appl. Crystallogr.*, 2009, **42**, 339.
47 K. Momma and F. Izumi, *J. Appl. Crystallogr.*, 2011, **44**, 1272.
48 J. Liu, C.-J. Yang, Q.-Y. Cao, M. Xu, J. Wang, H.-N. Peng, W.-F. Tan, X.-X. Lü and X.-C. Gao, *Inorg. Chim. Acta*, 2009, **362**, 575.
49 A. Díez, J. Forniés, S. Fuertes, E. Lalinde, C. Larraz, J. A. López, A. Martín, M. T. Moreno and V. Sicilia, *Organometallics*, 2009, **28**, 1705.
50 S. A. Katova, I. I. Eliseev, A. S. Mikherdov, E. V. Sokolova, G. L. Starova and M. A. Kinzhalov, *Russ. J. Gen. Chem.*, 2021, **91**(3), 430.